

Title:

Estimation of radioactivity in single photon emission computed tomography for sentinel lymph node biopsy in a torso phantom study

Running head:

Estimation of radioactivity of a small hot spot in SPECT images

Authors:

Hideaki Kitamura¹, Yuzuru Kono¹, Takeshi Murano¹, Kenta Hiroi¹, Kanyu Ihara¹, Tomohiko Aso¹, Kazumasa Inoue² and Masahiro Fukushi²

Affiliations:

¹Diagnosics Radiology Division, National Cancer Center Hospital, Tokyo, Japan

²Graduate School of Human Health Sciences, Tokyo Metropolitan University, Tokyo, Japan

Correspondence to: Hideaki Kitamura, Ph.D., R.T.

DiagnosicsRadiology Division

National Cancer Center Hospital

5-1-1 Tsukiji, chuo-ku, Tokyo, 104-0045 Japan

TEL: +81-3-3542-2511 FAX: +81-3-3545-3567

E-mail: hikitamu@ncc.go.jp

Acknowledgements:

This work was partially supported by Foundation for Promotion of Cancer Research.

Structured abstract

Objectives: Number of lymph nodes to be removed are determined from residual counts. Estimating residual radioactivity in lymphatic nodes before a biopsy in advance is useful for reducing surgical operation time. The purpose of this study was to estimate total radioactivity of a small hot spot in single-photon emission computed tomography (SPECT) of a torso phantom.

Methods: Cross-calibration study was performed to convert counts in SPECT images to radioactivity. A simulation study was performed to estimate the size of volume of interest (VOI) covering a hot spot corrupted with full width at half maximum (FWHM) between 8 and 16 mm. The estimation of total radioactivity was validated in a torso phantom study using small sources.

Results: True radioactivity was approximately equal to integrated values of hot spots using the VOI with a diameter of 40 mm in our simulation study. The difference was less than 18% in cases of more than 9.4 kBq.

Conclusions: The total radioactivity in small sources simulating a typical sentinel node was estimated from SPECT images using a VOI of 40 mm in a torso phantom study. Because the difference from actual values were less than 10% on average when radioactivities were more than 9.4 kBq, the total radioactivity of a lymph node can be estimated in a clinical examination.

Keywords

sentinel lymph node; total radioactivity; SPECT; quantification

Introduction

Sentinel lymph node (SLN) biopsy has been widely accepted as a method for staging regional lymph nodes for patients with melanoma [1-4]. The biopsy is performed by intradermal injection of a vital blue dye or a radioactive tracer, or both, around the melanoma. It has been demonstrated that use of the blue dye in combination with the radioactive tracer leads to optimal detection and identification of SLNs for melanoma.

Planar lymphoscintigraphy is routinely employed to visualize sentinel nodes and afferent lymphatic vessels preoperatively and to determine their number and location. However, single-photon emission computed tomography/computed tomography (SPECT/CT) has two advantages over planar lymphoscintigraphy. The tomographic nature of the technique and CT correction for attenuation and scatter of the gamma ray signals provide better sentinel node visualization [5]. Contamination, nodes close to the injection site, and overweight patients are noted instances in which SLNs are better identified and localized by SPECT/CT than planar lymphoscintigraphy in clinical situations [6-8]. After the SLN is identified through both in vivo imaging on a gamma camera and surveying with a gamma probe, a gamma probe is utilized to measure residual counts in the lymphatic nodes to identify and remove any additional hot lymph nodes [3, 9]. Therefore, lymph nodes that are to be removed are not determined from residual counts before surgical operations.

We have focused on estimating residual total radioactivity in lymphatic nodes, because it will reduce operation time if such lymph nodes are determined before a biopsy is performed. The radioactivity is calculated from voxel counts in SPECT images using a calibration factor obtained by imaging a phantom containing a known concentration of the same radionuclide used in clinical examination [10]. However, the quantitative accuracy of radioactivity measurements with SPECT can be compromised by partial volume error [11]. The poor spatial resolution of the SPECT imaging system causes a “spill-out” phenomenon. The sum of the intensities of all the voxels that is attributable to an object still reflects the total amount of radioactivity within it. However, the intensities of individual voxels no longer accurately reflect the concentration of the radioactivity contained within them. Therefore, total radioactivity can be measured by a volume of interest (VOI) of larger size as including spilled out intensity. However, if the total radioactivity is measured including radioactivity of other hot spots using oversized VOI, results in overestimated measurements. Therefore, accurate estimation needs to

determine appropriate VOI size according to the image resolution and SLNs size. The purpose of this study was to estimate the total radioactivity of a hot spot in SPECT images of a torso phantom using the VOI of size determined by a simulation study.

Materials and Methods

Image processing

SPECT/CT image data were acquired by Symbia T16 (Siemens AG, Medical Solutions, Erlangen, Germany). This system has a dual-head variable-head gamma camera equipped with low-energy low-penetration (LELP) collimators (21% window centered on the 140keV energy peak of Tc-99m) and a 16-multislice spiral CT component. The LELP collimators are specifically designed for lymphoscintigraphy to avoid “shine-through” artifacts from injection sites. The SPECT projection data (128×128 matrix, 30 frames) were acquired using 6° angular steps in a 16 s time frame throughout the study. In addition, the SPECT images (128×128 matrix; voxel size: $4.8 \text{ mm} \times 4.8 \text{ mm} \times 4.8 \text{ mm}$) were reconstructed with three-dimensional ordered subset expectation maximization including scatter correction with dual energy window method and CT-based attenuation correction using six subsets and eight iterations [12-14]. A CT scan with 130 kVp and 70 mAs using adaptive dose modulation (CARE Dose 4D) was performed subsequent to SPECT acquisition. The CT reconstruction used smooth and medium kernels (B8s and B40s, respectively) with a slice thickness of 3 mm.

Cross-calibration study

A cross-calibration study used a cylindrical phantom of a volume of 5640 mL (diameter, 200 mm; height, 200 mm). This phantom was filled with radioactivity concentrations of Tc-99m of 5.4, 15.5 and 44 MBq mL^{-1} and was scanned three times at the center of the field of view (FOV) with a 250-mm detector radius. Furthermore, the image processing described in Section “Image processing” was applied.

Average count values (M_{ave}) in the obtained SPECT images were measured in a 100-mm diameter region of interest at the center of the images with slice position between -48 and $+48$ mm so that the central axial FOV would be at a slice position of 0 mm. The cross-calibration factor (F_c) is expressed as follows:

$$Fc = \frac{C_{\text{phan}}}{M_{\text{ave}}/V_{\text{voxel}}}, \quad (1)$$

where C_{phan} BqmL⁻¹ denotes the radioactivity concentration in the cylindrical phantom, and V_{voxel} mL denotes the voxel volume, 0.11mL in this study.

Simulation study

We simulated a point spread function using a voxel size of 0.5 mm × 0.5 mm × 0.5 mm in image data with original programs (Visual Studio 2010 Professional, Microsoft). Uncorrupted sphere hot spots with a diameter of 2, 4, 6, 8 and 10 mm at the center of the images were convolved by a 3D-Gaussian kernel with an FWHM of 8, 10, 12, 14 and 16 mm. The images were simulated with no background activity. Integral in the simulated images were measured in spherical VOIs with a diameter of 10, 20, 30, 40, 50, 60 and 70 mm at the center of a hot spot. The totals were divided by the total value of the uncorrupted sphere hot spots in the simulated images according to FWHM, which values were UCRs. The VOI size was determined for a torso phantom study where these values were more than 95% in the simulation study.

Torso phantom study to validate estimation of radioactivity

The phantom study used a torso phantom (Kyotokagaku co, LTD, Japan) with small radioactive source inserts (a length of 5 mm × a diameter of 4 mm). The inserts contained Tc-99m with radioactivities between 1.7 kBq and 2.1 MBq to simulate clinical cases. They were inserted at specific positions to simulate an aortic bifurcation LN (A), an iliac LN (B), and an inguinal LN (C) in the torso phantom (Fig. 1). The inserted phantom was scanned three times at the center of the FOV. In addition, the image processing described in Section “Image processing” was applied with auto contouring for the distance between the phantom and detectors.

The total radioactivities were estimated using Fc within spherical VOIs with a diameter of 40 mm determined by the simulation study. The estimated radioactivities were compared with the true radioactivities in the inserted source as a relative difference. The relative difference D is defined as

$$D = \frac{A_e - A_t}{A_t} \times 100, \quad (2)$$

where A_e denotes the estimated radioactivity from the obtained SPECT images within VOIs, and

A_t denotes the actual (true) total radioactivity in the source insert. Then, the three calculated D values were averaged (D_{ave}) from repeated SPECT imaging data.

Results

Cross-calibration study

Fc was 14.4 ± 0.3 Bqcount⁻¹second⁻¹, using the torso phantom study.

Simulation study

The UCRs became larger with increasing VOI size, before reaching a plateau at a larger size (Fig. 2). The difference from an object size at an FWHM of 8 mm was greater in a 16 mm VOI than that in a smaller VOI size. The UCRs became larger than 0.95 when using a VOI 40 mm in diameter, when the spatial resolution was less than an FWHM of 16 mm, and the uncorrupted sphere hot spot was smaller than 10 mm.

Torso phantom study to validate estimation of radioactivity

All sources were depicted with a radioactivity level ranging between 9.4 kBq and 2.1 MBq. However, the source of position (A) was not depicted with a radioactivity of 5.7 kBq in two SPECT images of the three and was not depicted with a radioactivity of 1.7 kBq in any of the three images. The source of position (B) was also not depicted with a radioactivity of 5.7 kBq in one of the three images, nor with a radioactivity of 1.7 kBq in any of the images. The source of position (C) was depicted with a radioactivity of 5.5 kBq in all three images, but not depicted with a radioactivity of 1.7 kBq in one of three images.

The absolute values of D_{ave} showed less than 18% error in the radioactivities between 9.4 kBq and 2.1 MBq, and the absolute maximum value was 11% in radioactivities between 81 kBq and 2.1 MBq (Fig. 3). The D_{ave} values showed means of -9.2%, 0.96% and -0.085%, respectively, at (A), (B), and (C) in a radioactivity range 9.4 kBq–2.1 MBq. The D values showed a larger variance in the hot spots of all the positions having lower radioactivity levels.

Discussion

An object size of less than 10 mm was simulated in this simulation study because sentinel lymphoscintigraphy is not performed in lymphonodes larger than 10 mm, which are frequently

interpreted as metastases by other types of examination. The 3D-Gaussian filters used also simulated image resolution in a clinical SPECT image because its FWHM commonly ranges from 7 mm to 15 mm [15]. Therefore, we thought that the SLN hot spot was enclosed by a VOI 40 mm in diameter, including the counts spilled-out in a clinical examination, because this simulation study would be relevant for determining the VOI size. The estimation of radioactivity should use a controlled VOI size according to the amount of spill-out or the image resolution in a SPECT image. Its VOI size tended to be less dependent on the object size if the image resolution is low.

We believe this torso phantom study could be useful for simulating a patient with malignant melanoma of a lower extremity because a typical SLN ranges in size from 4 to 6 mm, the total radioactivity ranges from 1.1 to 1.8 MBq, and the absolute uptake in the surrounding tissues is extremely low [16, 17]. In addition, Renee et al. performed a torso phantom study simulating breast lymphoscintigraphy with a total activity in the node between 37 kBq and 370 kBq.

In the present study, the D_{ave} values were lower than 0% in the hot spot of (C) and were approximately 0% in the hot spots of (A) and (B), with radioactivity ranging between 9.4 kBq and 2.1 MBq. However, when the radioactivity was less than 5.5 kBq, either the hot spots were not depicted in the SPECT images or the estimation of radioactivity was inaccurate. Therefore, an accurate estimation of its radioactivity might be complicated.

Shcherbinin et al reported relative errors of approximately 5% while estimating total radioactivity in a phantom study. Furthermore, the results of our phantom study were quantitatively accurate and comparable to results obtained by other phantom studies [15, 18 and 19]. However, in our study, the relative error of estimation was greater at radioactivities between 9.4 and 27 kBq because the size of the inserted radioactivity sources was smaller and the filled radioactivities were lower. The error of estimation would depend on the accuracy of the attenuation and scatter correction [20]. Moreover, the precision of estimation was reduced as the radioactivity of the inserted sources decreased because the statistical error was increasing as the detected counts were decreasing.

The present study has several limitations; spill-in from injection sites were not taken into account. Therefore, we believe that the overall accuracy should be assessed in a clinical study. The estimation of radioactivity would be overestimated in the presence of other hot spots around the estimated SLN because of the effect of spilled-in counts from hot spots. However,

this effect can be decreased if the VOI size covering the corrupted hot spot is decreased by spatial resolution correction processing. Thus, it is possible to estimate the total radioactivity of a lymph node consuming more than approximately 10 kBq in a clinical examination. Therefore, unnecessary biopsy procedures might be avoided because of preoperative identification of SLNs to perform.

In conclusion, the total radioactivity in small sources simulating a typical sentinel node was estimated from SPECT images using a VOI with a diameter of 40 mm in a torso phantom study. Because the difference from actual values were less than 10% on average when radioactivities were more than 9.4 kBq, the total radioactivity of a lymph node can be estimated in a clinical examination.

References

- 1 Wong SL, Balch CM, Hurley P, Agarwala SS, Akhurst TJ, Cochran A, *et al.* Sentinel lymph node biopsy for melanoma: American Society of Clinical Oncology and Society of Surgical Oncology joint clinical practice guideline. *J Clin Oncol* 2012; **30**: 2912–2918.
- 2 Ho Shon IA, Chung DK, Saw RP, Thompson JF. Imaging in cutaneous melanoma. *Nucl Med Commun* 2008; **29**: 847-76.
- 3 Mariani G, Erba P, Manca G, Villa G, Gipponi M, Boni G, *et al.* Radioguided sentinel lymph node biopsy in malignant cutaneous melanoma. *J Nucl Med* 2002; **43**: 811–827.
- 4 Vermeeren L, van der Ploeg IM, Olmos RA, Meinhardt W, Klop WM, Kroon BB, *et al.* SPECT/CT for preoperative sentinel node localization. *J Surg Oncol* 2010; **101**: 184–190.
- 5 Seo Y, Mari C, Hasegawa BH. Technological development and advances in single-photon emission computed tomography/computed tomography. *Semin Nucl Med* 2008; **38**: 177–198.
- 6 Vermeeren L, Valdés Olmos RA, Klop WM, van der Ploeg IM, Nieweg OE, Balm AJ, *et al.* SPECT/CT for sentinel lymph node mapping in head and neck melanoma. *Head Neck* 2011; **33**: 1–6.
- 7 van der Ploeg IM, Valdés Olmos RA, Nieweg OE, Rutgers EJ, Kroon BB, Hoefnagel CA. The additional value of SPECT/CT in lymphatic mapping in breast cancer and melanoma. *J Nucl Med* 2007; **48**: 1756–1760.

- 8 Wagner T, Buscombe J, Gnanasegaran G, Navalkissoor S. SPECT/CT in sentinel node imaging. *Nucl Med Commun* 2013; **34**: 191-202.
- 9 McMasters KM, Reintgen DS, Ross MI, Wong SL, Gershenwald JE, Krag DN, *et al.* Sentinel lymph node biopsy for melanoma: how many radioactive nodes should be removed? *Ann Surg Oncol* 2001; **8**: 192–197.
- 10 Zeintl J, Vija AH, Yahil A, Hornegger J, Kuwert T. Quantitative accuracy of clinical ^{99m}Tc SPECT/CT using ordered-subset expectation maximization with 3-dimensional resolution recovery, attenuation, and scatter correction. *J Nucl Med* 2010; **51**: 921–928.
- 11 Ralph A. B, Sibylle I. Z. Basics of PET and SPECT Imaging. In: Mohammad D, Xiaoyi J, Klaus S, eds. Correction techniques in emission tomography. New York: CRC Press, 2012: 51–64.
- 12 Gantet P, Payoux P, Celler A, Majorel C, Gourion D, Noll D, *et al.* Iterative three-dimensional expectation maximization restoration of single photon emission computed tomography images: application in striatal imaging. *Med Phys* 2006; **33**: 52–60.
- 13 James A. Patton, Timothy G. Turkington. SPECT/CT Physical Principles and Attenuation Correction. *J Nucl Med Technol* 2008; **36**: 1–10.
- 14 Zaidi H, Hasegawa B. Determination of the attenuation map in emission tomography. *J Nucl Med* 2003; **44**: 291–315.
- 15 Philipp Ritt, Hans Vija, Joachim Hornegger, Torsten Kuwert. Absolute quantification in SPECT. *Eur J Nucl Med Mol Imaging* 2011; **38**: 69–77.
- 16 Dickinson RL, Erwin WD, Stevens DM, Bidaut LM, Mar MV, Macapinlac HA, *et al.* Hybrid Modality Fusion of Planar Scintigrams and CT Topograms to Localize Sentinel Lymph Nodes in Breast Lymphoscintigraphy: Technical Description and Phantom Studies. *Int J Mol Imaging* 2011; 1–10.
- 17 Kapteijn BA, Nieweg OE, Muller SH, Liem IH, Hoefnagel CA, Rutgers EJ, *et al.* Validation of gamma probe detection of the sentinel node in melanoma. *J Nucl Med* 1997; **38**: 362–366.
- 18 S Shcherbinin, A Celler, T Belhocine, R Vanderwerf, A Driedger. Accuracy of quantitative reconstructions in SPECT/CT imaging. *Phys Med Biol* 2008; **53**: 4595–4604.
- 19 Kathy Willowson, Dale L Bailey, Clive Baldock. Quantitative SPECT reconstruction using CT-derived corrections. *Phys Med Biol* 2008; **53**: 3099–3112.

- 20 Patton JA, Turkington TG. SPECT/CT physical principles and attenuation correction. *J Nucl Med Technol* 2008; **36**: 1-10.

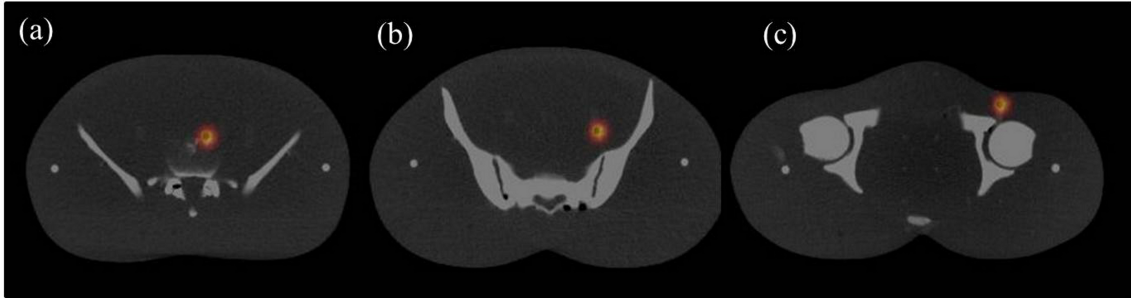


Figure 1. The positions of source inserts in the torso phantom.

(a), (b), and (c) denote the positions of sources simulated an aortic bifurcation LN (A), an iliac LN (B), and an inguinal LN (C) in the phantom.

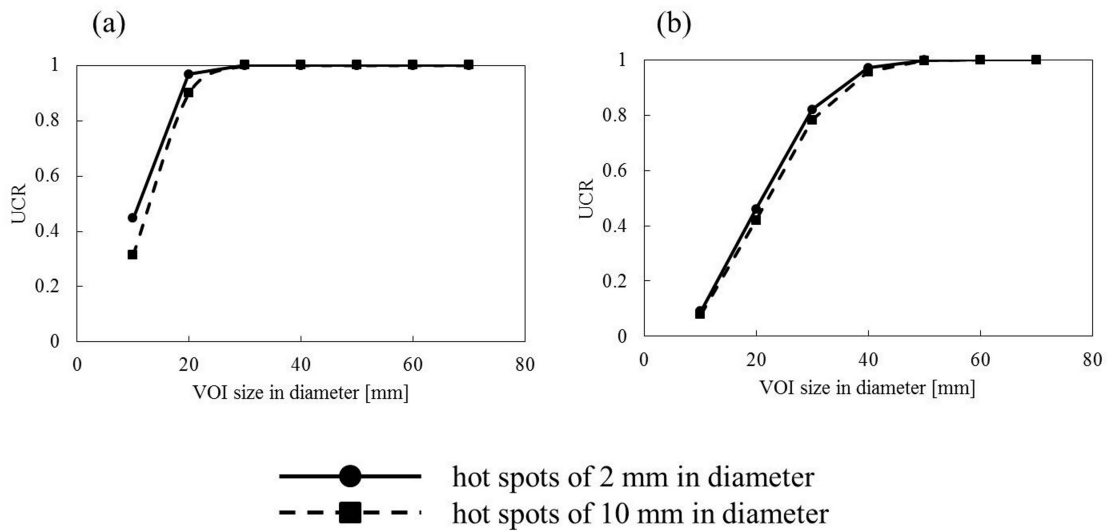


Figure 2. UCRs as function of VOI volumes for FWHM of 3D-Gaussian kernel.

UCR is 1.0 when the total voxel value of hot spot is equal to the value integrated inside a VOI. (a) and (b) denote uncorrupted sphere hot spots were convolved by a 3D-Gaussian kernel with an FWHM of 8 and 16 mm, respectively.

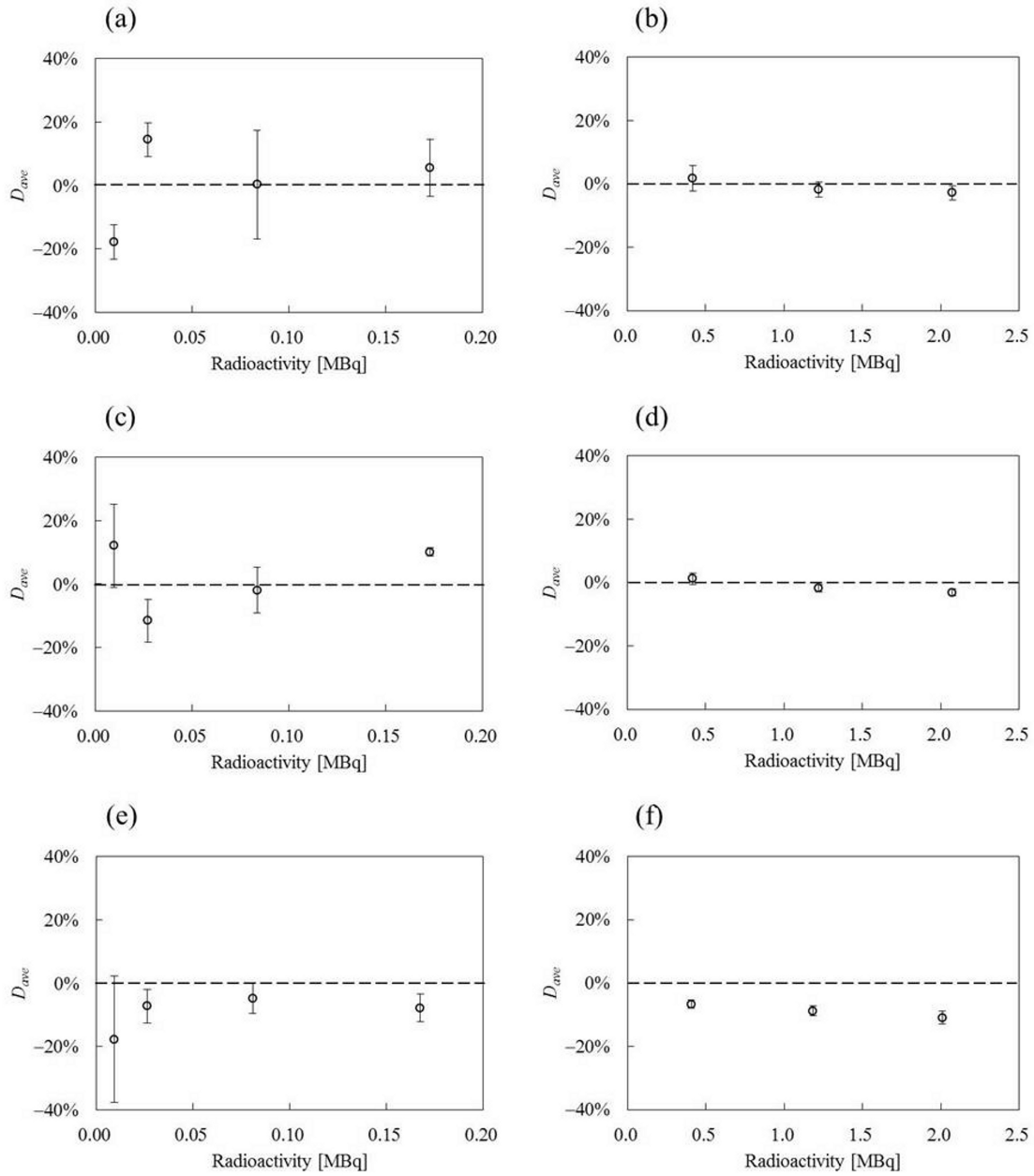


Figure 3. D_{ave} as a function of radioactivity of the inserted sources.

Dashed lines denote a D_{ave} of 0%. (a) and (b) denote a position (A) in radioactivities ranging from 9.7 kBq to 0.17 MBq and ranging from 0.42 MBq to 2.1 MBq, respectively. (c) and (d) denote a position (B) in radioactivities ranging from 9.7 kBq to 0.17 MBq and ranging from 0.42 MBq to 2.1 MBq. (e) and (f) denote a position (C) in radioactivities ranging from 9.4 kBq to 0.17 MBq and ranging from 0.41 MBq to 2.0 MBq.